RSC Advances

PAPER

View Article Online
View Journal | View Issue

Cite this: *RSC Adv.*, 2025, **15**, 33131

Investigation of the structural, electronic and optical properties of $C_9H_{17}NO_2$ phases with promising potential for optoelectronic devices

Faisal Katib Alanazi,*[a] K. Bouferrache,[bc] Maroua I. Benamrani,[d] Rabah Boudissa,[b] M. Fatmi *[b] and M. A. Ghebouli[be]

Received 17th May 2025
Accepted 27th August 2025

DOI: 10.1039/d5ra03480a

rsc.li/rsc-advances

Gabapentin ($C_9H_{17}NO_2$) is a small organic molecule known for its pharmaceutical use, but in its solid-state crystalline forms, it exhibits promising structural and optoelectronic properties. In this work, we employed density functional theory (DFT) to investigate the structural, electronic, and optical properties of three anhydrous polymorphs (α, β, and γ) of gabapentin. The calculated band gaps for the α, β, and γ polymorphs of $C_9H_{17}NO_2$ were found to be 4.73 eV, 4.55 eV, and 4.37 eV, respectively, based on GGA-PBE. To improve the accuracy, we also used the mBJ-GGA method, which yielded band gaps of 5.5 eV, 5.1 eV, and 5.9 eV, respectively, and these values indicated that all the three phases absorb in the ultraviolet (UV) region. Additionally, the static dielectric constants were calculated to be 2.64, 2.57, and 2.40, respectively, confirming their excellent insulating properties. These results highlight the potential of gabapentin polymorphs for UV optoelectronic applications such as UV detectors, reflective coatings, and high-frequency insulators.

1. Introduction

Frequency-dependent dielectric properties can be used to characterize biological materials and determine the formation of new phases from biological processes. Although generally inaccessible *via* experimental methods, computer simulations can be used to determine the dielectric properties of biological materials. In some studies, the dielectric constant is defined as the static dielectric constant of the material, which is not accurate because it does not give precise results on the dielectric properties. Electrical insulators are also known as dielectric materials and are characterized by the absence of free charge carriers capable of conducting electrons. Insulators or dielectrics are materials with a very high resistivity in the range of 10^8 to 10^{16} Ω m because they contain very few free electrons.[1,2] In a dielectric, the atoms strongly retain their electrons. The most abundant elements are the atoms of carbon (C), hydrogen (H), oxygen (O) and nitrogen (N), which alone constitute 96% of living matter. In smaller amounts, phosphorus (P) and sulfur (S) are also present. Gabapentin ($C_9H_{17}NO_2$) is a biological compound whose crystal structure, in the solid state, exists in three polymorphic forms (α, β, and γ), as illustrated in Fig. 1. Hayley *et al.*[3] studied the α-gabapentin polymorph and compared it with the data reported by Ibers.[4] Initially, gabapentin was developed as an antiepileptic drug; however, its applications were later extended to the treatment of neuropathic pain.[5] L. Magnus[5] demonstrated that gabapentin is useful in neuropathic pain syndromes, bipolar disorders, movement disorders, migraine prophylaxis and cocaine dependence. On the other hand, gabapentin is an insulator with band gap close to 5 eV. We know that insulating materials find applications in a large number of devices for the production, transport, distribution and use of electrical energy. An insulating material is a material intended to prevent electrical conduction between conductive elements. It is a material with very low, practically negligible electrical conductivity, used to separate conductive parts maintained at different potentials. The use of such materials is expanding beyond electrical engineering to various other fields, including aeronautics, automobile manufacturing, construction, and even medicine. The use of more efficient materials, such as wide-band-gap semiconductors (SC2G), is therefore increasingly being considered for high-power (HP) and high-frequency (HF) applications. The intrinsic properties of SC2G make them well-suited materials for HP, HF, and HV electronics. The most remarkable optical property of this family of semiconductors is their wide band gap. Lighting technology experienced a spectacular revolution with the manufacture of LEDs (light emitting diodes), which are

[a]*Department of Physics, College of Sciences, Northern Border University, P.O. Box 1321, 91431 Arar, Saudi Arabia. E-mail: faisal.katib.al@gmail.com*

[b]*Research Unit on Emerging Materials (RUEM), University Ferhat Abbas of Setif 1, Setif, 19000, Algeria*

[c]*Department of Physics, Faculty of Sciences, University of M'sila University Pole, Road Bourdj Bou Arreiridj, M'sila, 28000, Algeria*

[d]*Laboratoire de Croissance et Caractérisation de Nouveaux Semiconducteurs (LCCNS), Faculté de Technologie, Université Ferhat Abbas Setif 1, 19000 Setif, Algeria*

[e]*Department of Chemistry, Faculty of Sciences, University of M'sila University Pole, Road Bourdj Bou Arreiridj, M'sila, 28000, Algeria*

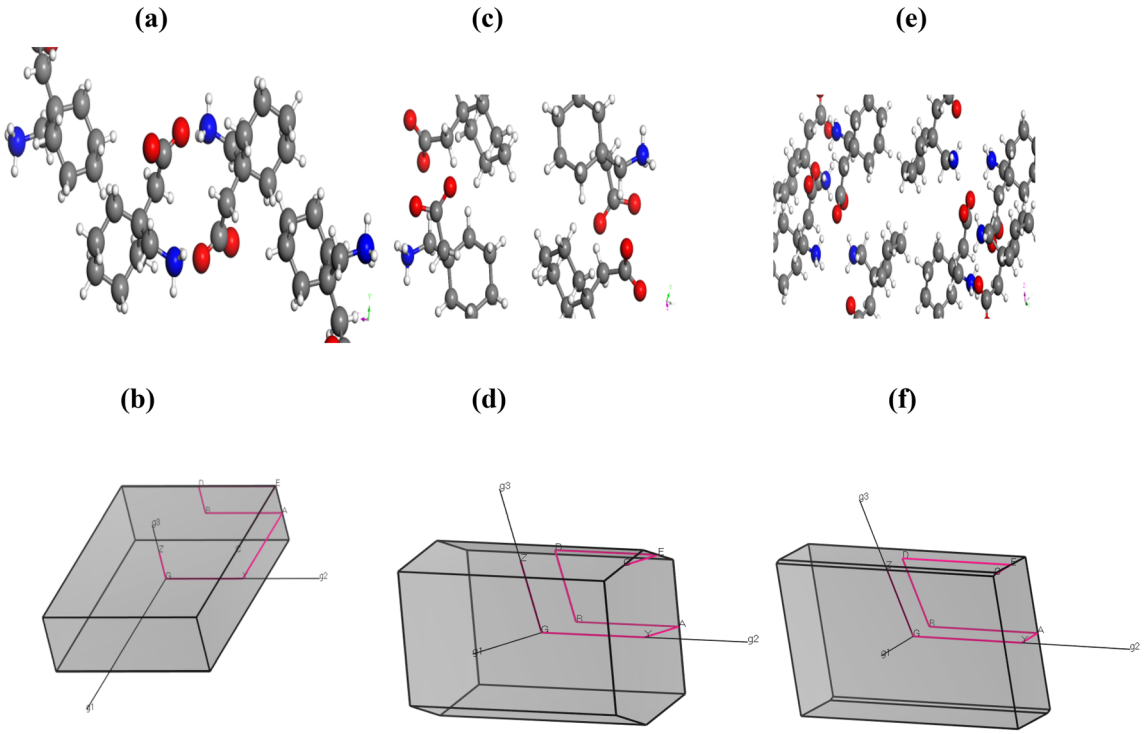

Fig. 1 2D and 3D representations of the three polymorphs: (α) gabapentin (a and b), (β) gabapentin (c and d) and (γ) gabapentin (e and f).

devices based on nitride-type semiconductors. This was made possible by manufacturing LEDs that emit blue light. There are materials that may possess a band gap as high as 6 eV, and it appears that there is a particular difference in their electrical insulation and thermal conductivity. The insulators that have significantly wider energy band gaps include SiO_2 with a band gap of 9.0 eV,[6] which on the other hand has a refractive index of 1.46 and presents good transparency under visible light; diamond, given its high carbon–carbon covalent bond energy, with a band gap of 5.47 eV;[7,8] silicon nitride (Si_3N_4) with an index of 2.02 and a mediocre dielectric ($E_g \sim 5.5$ eV);[9] and finally, aluminum nitride (AlN), a III–V semiconductor, with a direct gap of 6.015 eV[10] at 300 K. Similar to electrical insulators, aluminum nitride (AlN), although a refractory ceramic, has the peculiarity of being both an electrical insulator and a thermal conductor, with very high thermal conductivity reaching up to 285 w m^{-1} K^{-1} depending on the structure of the material, such as a single crystal,[11] which is characterized by a dielectric constant close to 8, a low coefficient of thermal expansion of 4×10^{-6} $°C^{-1}$, close to good dielectric resistivity, good insulation and good mechanical resistance. This unusual combination of properties makes AlN a magnificent material for many applications in optics, lighting, electronics and renewable energy. Our compound, being an electrical insulator similar to aluminum nitride, shows potential for applications as a substrate for epitaxial growth in ultraviolet (UV) optoelectronics and for the fabrication of microwave power transistors in power electronics. Currently, much research is being carried out to produce UV-emitting light-emitting diodes (LEDs) using aluminum-gallium nitride. On the other side, materials having a band gap width of $0 < E_g < 5$ eV are called intrinsic semiconductors. They are characterized by a resistivity much higher than that of a good conductor and much lower than that of a good insulator. Based on its wide band gap, excellent dielectric properties, and strong absorption in the ultraviolet region, the $C_9H_{17}NO_2$ compound (gabapentin polymorphs) demonstrates promising potential for applications in optoelectronic devices, such as UV detectors and emitters, high-power and high-frequency electronic insulation systems, and reflective UV coatings, and as a substrate material for epitaxial growth in semiconductor technologies. Furthermore, recent studies have shown increasing interest in wide band gap semiconductors for advanced applications in spintronics and valvetrains, highlighting the broader impact of such materials beyond traditional electronics and optics.[12,13] The objective of this work is to achieve a comprehensive understanding of the structural, electronic, and optical properties of $C_9H_{17}NO_2$ at the atomistic level.

2. Computational details

All calculations were performed using the CASTEP code,[14] which implements density functional theory (DFT) with a plane-wave basis set and a pseudo-potential approach. The exchange-correlation effects were treated using GGA-PBE96.[15] The ionic cores were represented by Norm conserving pseudopotentials[16] for H, C, N and O. The H $1s^1$, C $2s^2 2p^2$, N $2s^2 2p^3$ and O $2s^2 2p^4$ orbitals were treated as valence electrons. A plane-wave basis set cut-off of 830 eV and a Monkhorst Pack mesh[17] of $4 \times 4 \times 4$ for the k points were chosen after a convergence test to ensure

sufficiently accurate calculations. Within a density mixing system, the atomic locations were optimized and relaxed using a conjugate gradient (CG) approach for eigenvalue minimization. In this work, hydrostatic pressure was applied during geometry optimization using the CASTEP code. The external pressure was set directly in the calculation input, ranging from 0 to 5 GPa, allowing the unit cell to fully relax under an isotropic stress condition. In reality, a structural optimization employing the Broyden–Fletcher–Goldfarb–Shenno (BFGS) minimization technique yielded the equilibrium lattice parameter. With the following thresholds for convergent structures, this method offers a quick way to identify the lowest energy structure:

(i) Energy change per atom of less than 5×10^{-6} eV,

(ii) Residual force of less than 0.01 eV Å^{-1},

(iii) Atom displacement during geometry optimization of less than 0.0005 Å, and

(iv) Maximum stress of 0.02 GPa.

3. Results and discussions

3.1. Structural properties

The crystal structures of (α, β, γ)-$C_9H_{17}NO_2$ are monoclinic belonging to the space groups of $P2_1/c$ (N°14), $P2_1/c$ (N°14), and $C2/c$ (N°15), respectively. The calculated structural parameters a, b, and c show acceptable agreement with the experimental data,[3,4,18] as presented in Table 1. The calculated ratios c/a and c/b also match well with the reference values. The molecular and crystal structures of the three polymorphs, (α, β, γ)-$C_9H_{17}NO_2$, in both 2D and 3D representations are illustrated in Fig. 1. These visualizations help to highlight the symmetry differences among the three phases. The α-phase has the most elongated structure (c/a = 3.78), indicating strong intermolecular hydrogen bonding along the c-axis. The β-phase shows an intermediate packing efficiency with $\beta = 106.189°$, suggesting moderate intermolecular interactions. The γ-phase exhibits the highest packing density (1.156 g cm^{-3}) and the largest unit cell volume, indicating an optimal space utilization. The calculated formation enthalpies reveal that the γ-phase is thermodynamically the most stable (−22395.74 eV), followed by α (−11197.78 eV) and β (−11197.60 eV). This stability order correlates with the observed packing efficiency, where tighter molecular arrangements in the γ-phase lead to stronger intermolecular forces and enhanced stability.

3.2. Electronic properties

The electronic band dispersions of monoclinic (α, β, γ)-$C_9H_{17}NO_2$ are plotted in Fig. 2, along with the high symmetry lines inside the irreducible Brillouin zone (IBZ). Crystal structure optimization shows semiconductor properties with an indirect band gap for (α, β, γ)-$C_9H_{17}NO_2$ and a fundamental band gap of 4.731 eV for alpha, 4.555 eV for beta, and 4.371 eV for gamma phases. Similar to α-$C_9H_{17}NO_2$, monoclinic β-$C_9H_{17}NO_2$ and γ-$C_9H_{17}NO_2$ also exhibit an indirect band gap semiconductor behavior with a larger fundamental band gap of 4.371 eV. The valence band maximum (VBM) and conduction band minimum (CBM) occur at the B-D and Γ symmetry points in α-$C_9H_{17}NO_2$, while they appear at Y-A and Γ in β-$C_9H_{17}NO_2$ and at A and Γ in γ-$C_9H_{17}NO_2$ symmetry points of the irreducible Brillouin zone (IBZ). The band gaps of the (α, β, γ)-$C_9H_{17}NO_2$ compounds are found to be 4.88 eV, 4.83 eV and 5.39 eV respectively. To improve the accuracy of the band gap predictions beyond the standard GGA-PBE, additional calculations are carried out using the modified Becke–Johnson potential (mBJ-GGA).[19] This semi-local approximation is known for providing more accurate estimates of band gaps in wide band gap materials. The obtained values are 5.5 eV for α-$C_9H_{17}NO_2$, 5.1 eV for β-$C_9H_{17}NO_2$, and 5.9 eV for γ-$C_9H_{17}NO_2$. These results confirm the classification of the studied polymorphs as wide band gap materials with strong absorption in the ultraviolet region, reinforcing their potential for

Table 1 Experimentally observed cell parameters of (α, β, γ)-$C_9H_{17}NO_2$ (in parentheses) and the corresponding calculated values

Common name	α-Gabapentin 4	β-Gabapentin 3	γ-Gabapentin 18
Chemical formula	$C_{36}H_{68}N_4O_8$	$C_{36}H_{68}N_4O_8$	$C_{36}H_{68}N_4O_8$
a (Å)	5.9826 (5.8759)	14.7719 (14.5376)	30.6099 (30.5452)
b (Å)	7.0155 (6.9198)	6.7488 (6.6329) Å	6.0906 (5.9268)
c (Å)	22.6090 (22.2620)	10.0169 (9.8343) Å	11.1265 (10.8841)
$\Delta a/a$%	1.8	1.6	0.21
$\Delta b/b$%	1.4	1.4	2.7
$\Delta c/c$%	1.5	1.8	2.2
c/a	3.7791 (3.788)	0.6781 (0.665)	0.3635 (0.356)
c/b	3.2227 (3.217)	1.4842 (1.482)	1.8268 (1.836)
α	90° (90°)	90° (90°)	90° (90°)
β	90 181 (90.080°)	106.189° (105.922°)	108.1880 (108.316)
$\Delta\beta/\beta$%	0.11	0.25	0.11
γ	90° (90°)	90° (90°)	90° (90°)
Cell volume (Å^3)	948 681 (905.173)	959.02 (911.91)	1970.74 (1870.58)
Density(g cm^{-3})	1.18160	1.17596	1.15585
Number of distinct elements	4 (4)	4 (4)	8 (8)
Space group number	14	14	15
Space group (monoclinic)	$P2_1/c$	$P2_1/c$	$C2/c$
H (eV)	−11197.78	−11197.60	−22395.74

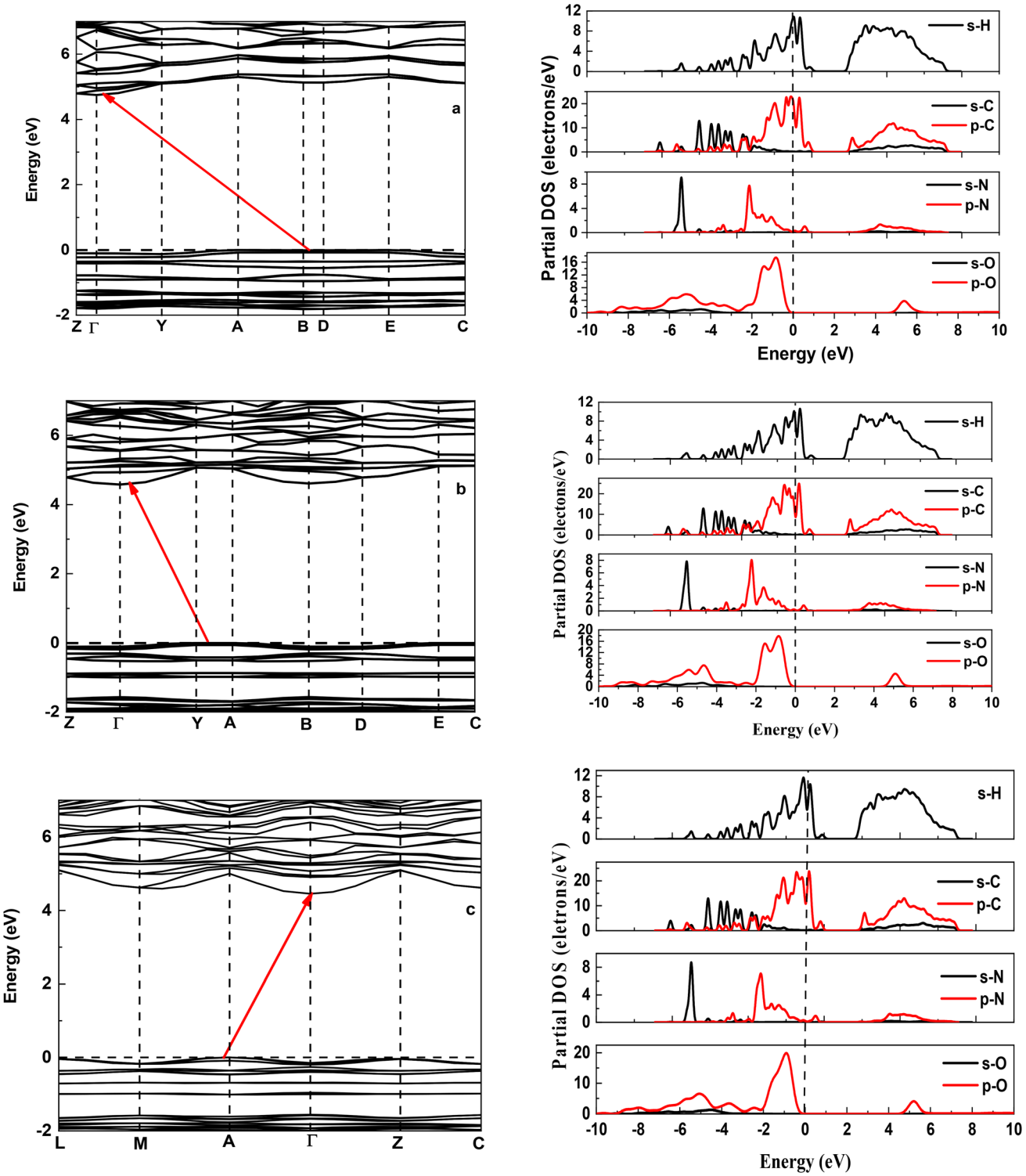

Fig. 2 Band structure and PDOS of the three polymorphs: (α) gabapentin (a), (β) gabapentin (b) and (γ) gabapentin (c).

optoelectronic and UV device applications. The decreasing band gap trend ($\alpha > \beta > \gamma$) correlates inversely with the structural stability. This phenomenon occurs because intermolecular π–π interactions in the more stable γ-phase create additional electronic states that slightly narrow the band gap, and molecular orbital overlap increases with packing density, leading to band dispersion. The partial density of states (PDOS) provided more information about the band structure of the (α, β, γ)-$C_9H_{17}NO_2$ compounds. The partial DOS confirms that the top of the valence bands of the compounds primarily originates from the O-2p orbitals, and the bottom of the conduction band comes mainly from the C-2p orbitals, with weak contributions

from the H-1s orbitals. The valence band of the (α, β, γ)-$C_9H_{17}NO_2$ compounds is divided into three distinct regions: the energy region from −22.0 eV to ∼−18.0 eV, dominated by the 2s/2s orbitals of the N and O atoms, with small contributions from the H-1s orbital; the energy region from −18.0 eV to ∼−10.0 eV, dominated by the 2p/1s orbitals of the C and H atoms, with small contributions from the N-2p orbitals; and the energy region from −10.0 eV to ∼0.0 eV, dominated by the 2p/1s orbitals of the C, O and H atoms, with small contributions from the N-2p orbitals. The 1s/2p orbitals of the H/O atoms of the (α, β, γ)-$C_9H_{17}NO_2$ compounds present strong interactions with each other from −10.0 eV to ∼0.0 eV. However, the 2s/1s orbitals of the C/H atoms (from −18.0 eV to ∼−10.0 eV) in (α, β, γ)-$C_9H_{17}NO_2$ interact only partially.

3.3. Optical properties

The study of the optical properties of a compound is necessary to obtain a clear idea of its electronic structure. To do that, let us consider different photon energies to calculate some optical properties of the monoclinic (α, β, γ)-$C_9H_{17}NO_2$crystals. For an incident light polarized in the [100] direction, the dielectric function $\varepsilon(\omega)$ is initially calculated, which is the fundamental optical parameter that describes the optical properties of a material. $\varepsilon(\omega)$ describes the relationship between the real part and the imaginary part of the dielectric function as $\varepsilon(\omega) = \varepsilon_1(\omega) + i\varepsilon_2(\omega)$, where $\varepsilon_1(\omega)$ is the real part (absorption) and $\varepsilon_2(\omega)$ is the imaginary part (polarization) of the dielectric function. Semiconductors play a key role in the production of information and communication technologies and constitute the basic components of these technologies. A dielectric is defined as a material medium in which the conduction and valence bands are separated by an energy gap greater than 5 eV. By linear response formalism, the calculated real part of the dielectric function ε_1, which describes the electronic polarizability, is extracted from the imaginary part of the dielectric function using the Kramers–Kronig expression. The ε_1 shows maxima at (5.55 eV, 7.65 eV), (5.54 eV, 8.17 eV) for (α, β)-$C_9H_{17}NO_2$) and 8.64 eV for (γ)-$C_9H_{17}NO_2$). The real part of the dielectric function, $\varepsilon_1(\omega)$, is positive up to 15.44 eV, 14.54 eV, and 13.88 eV for the respective phases, but turns negative at higher energies. For α-, β-, and γ-$C_9H_{17}NO_2$, the plasma frequencies are observed at (15.44, 22.09 eV), (14.54, 21.63 eV), and (13.88, 21.15 eV), respectively. The static values of the real part of the dielectric function, $\varepsilon_1(0)$, are 2.64, 2.57, and 2.40 for the α, β, and γ phases, respectively (Fig. 3). The imaginary part $\varepsilon_2(\omega)$ of the dielectric function $\varepsilon(\omega)$ can be obtained from the momentum matrix between the occupied and unoccupied electronic states:[20]

$$\varepsilon_2(\omega) = \frac{2\omega^2\pi}{V\varepsilon_0}\sum_{k,v,c}|\langle\psi_k{}^c|u.r|\psi_v{}^c\rangle|^2\delta(E_k{}^c - E_k{}^v - \hbar\omega) \quad (1)$$

where u is the vector that provides the polarization of the electric field of the incident electromagnetic radiation, V is the volume of the unit cell, and $\psi_k{}^c$ represents the wave function of the valence (conduction) band at the wave vector k, according to the Kramers–Kronig relations.[21–23]

$$\varepsilon_1(\omega) = 1 + \frac{2}{\pi}P\int_0^\infty \frac{\omega'\varepsilon_2(\omega')}{\omega'^2 - \omega^2}\mathrm{d}\omega' \quad (2)$$

$$n(\omega) = \frac{1}{\sqrt{2}}\left[\sqrt{\varepsilon_1{}^2(\omega) + \varepsilon_2{}^2(\omega)} + \varepsilon_1(\omega)\right]^{\frac{1}{2}} \sigma(\omega) = \frac{\omega\varepsilon_2}{4\pi} \quad (3)$$

$$\alpha(\omega) = \sqrt{2}\omega\left[\sqrt{\varepsilon_1{}^2(\omega) + \varepsilon_2{}^2(\omega)} + \varepsilon_1(\omega)\right]^{\frac{1}{2}} \quad (4)$$

$$R(\omega) = \left|\frac{\sqrt{\varepsilon(\omega)} - 1}{\sqrt{\varepsilon(\omega)} + 1}\right|^2 \quad (5)$$

$$L(\omega) = \frac{\varepsilon_2(\omega)}{\varepsilon_1{}^2(\omega) + \varepsilon_2{}^2(\omega)} \quad (6)$$

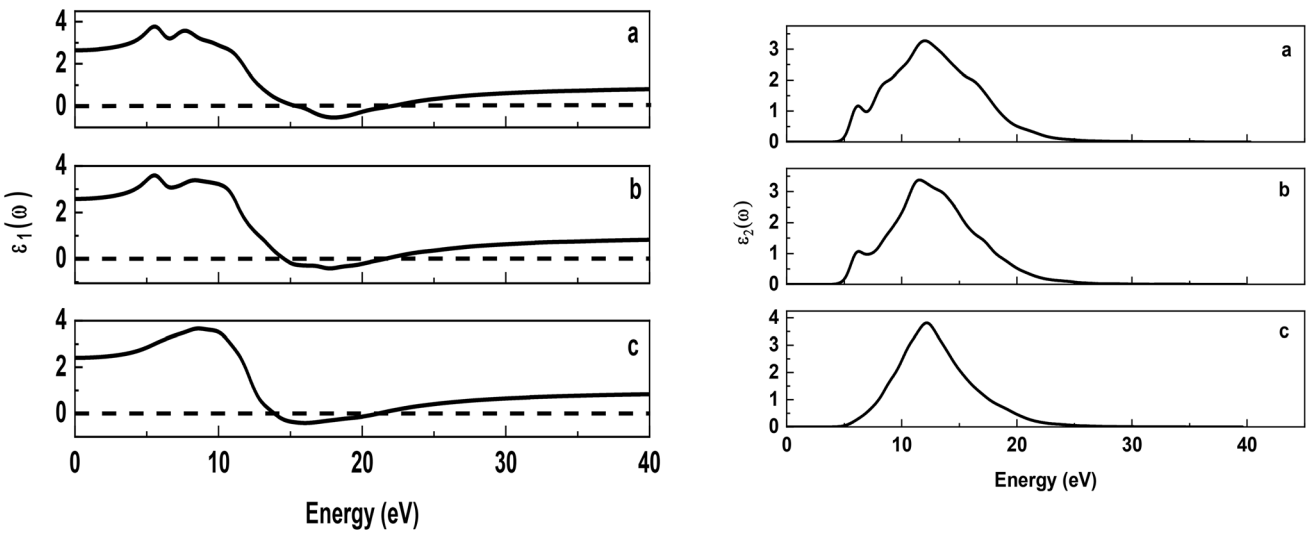

Fig. 3 Real and imaginary parts of the dielectric function of the three polymorphs: (α) gabapentin (a), (β) gabapentin (b) and (γ) gabapentin (c).

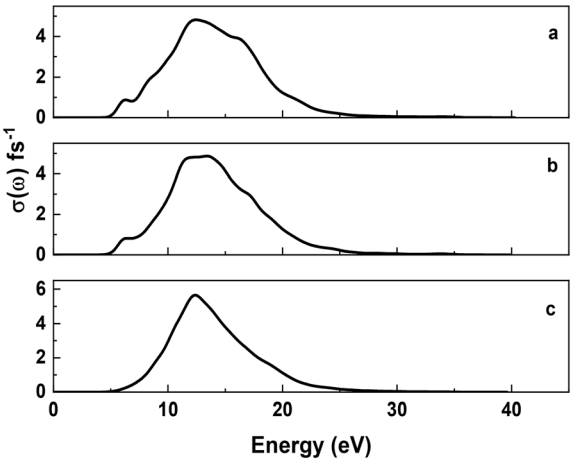

Fig. 4 Optical conductivity function of the three polymorphs: (α) gabapentin (a), (β) gabapentin (b) and (γ) gabapentin (c).

In the (α, β, γ)-$C_9H_{17}NO_2$ phases, the threshold energies are 4.40 eV, 4.15 eV, and 4.58 eV, respectively. The absorption peaks are located at 6.21 eV and 12.04 eV for α-$C_9H_{17}NO_2$, at 6.28 eV and 11.51 eV for β-$C_9H_{17}NO_2$, and at 12.17 eV for γ-$C_9H_{17}NO_2$. The observed difference in the absorption peaks is attributed to their different crystal structures. On the basis of the dielectric function, the $\sigma(\omega)$ component of the optical conductivity is calculated for the compounds (Fig. 4). For (α, β, γ)-$C_9H_{17}NO_2$, the maximum values of $\sigma(\omega)$ are situated around 6.29 eV (0.88 fs^{-1}), 12.46 eV (4.82 fs^{-1}), 6.43 eV (0.82 fs^{-1}), 13.42 eV (4.87 fs^{-1}) and 12.41 eV (5.66 fs^{-1}). The theoretical spectra of the energy loss function $L(\omega)$ for the (α, β, γ)-$C_9H_{17}NO_2$ compounds are shown in Fig. 5. These features are responsible for the plasmon resonance in $L(\omega)$, with the first peak appearing similarly along both crystal directions. The theoretical spectrum $L(\omega)$ shows similar features at 22.43 eV, 22.01 eV and 21.55 eV for the (α, β, γ)-$C_9H_{17}NO_2$ compounds, respectively; in this regard no experimental results are available for comparison. The region of the electromagnetic spectrum in which the material absorbs energy is indicated by its absorption coefficient, which also provides vital information on the conversion of solar energy. Fig. 6 shows

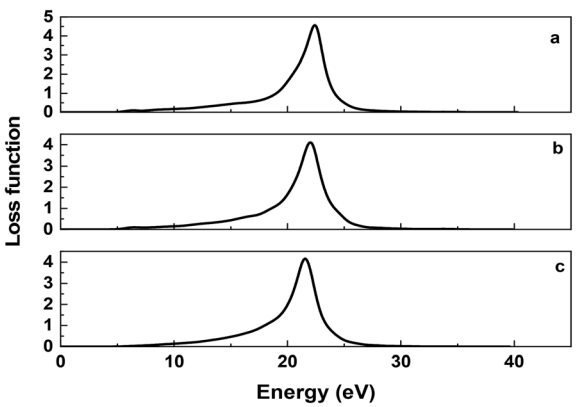

Fig. 5 Energy loss function of the three polymorphs: (α) gabapentin (a), (β) gabapentin (b) and (γ) gabapentin (c).

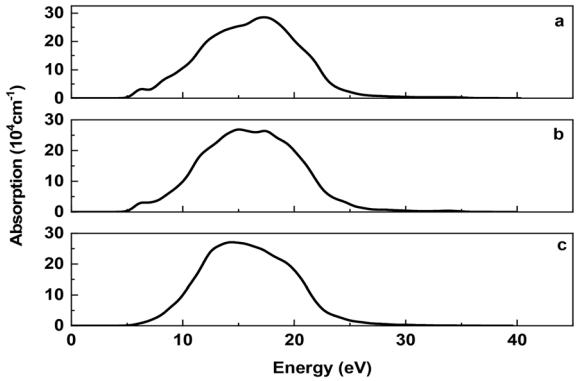

Fig. 6 Absorption spectra of the three polymorphs: (α) gabapentin (a), (β) gabapentin (b) and (γ) gabapentin (c).

the optical absorption spectra of the alpha-, beta- and gamma-crystal polymorphs of gabapentin along the [100] polarization direction. Therefore, the obtained results indicate that the gabapentin crystals in these three phases absorb in the ultra violet (UV) region with absorption maxima at 17.25 eV, 15.00 eV and 14.29 eV (28.53×10^4, 26.83×10^4 and 27.07×10^4),

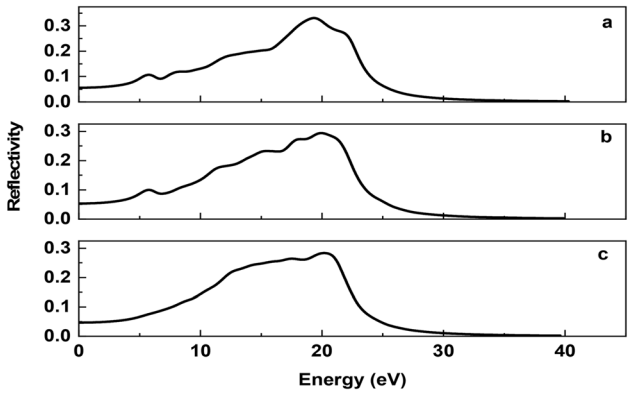

Fig. 7 Reflectivity spectra of the three polymorphs: (α) gabapentin (a), (β) gabapentin (b) and (γ) gabapentin (c).

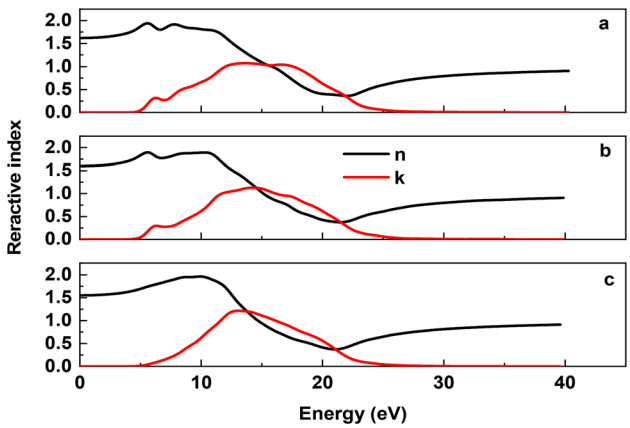

Fig. 8 Refractive index of the three polymorphs: (α) gabapentin (a), (β) gabapentin (b) and (γ) gabapentin (c).

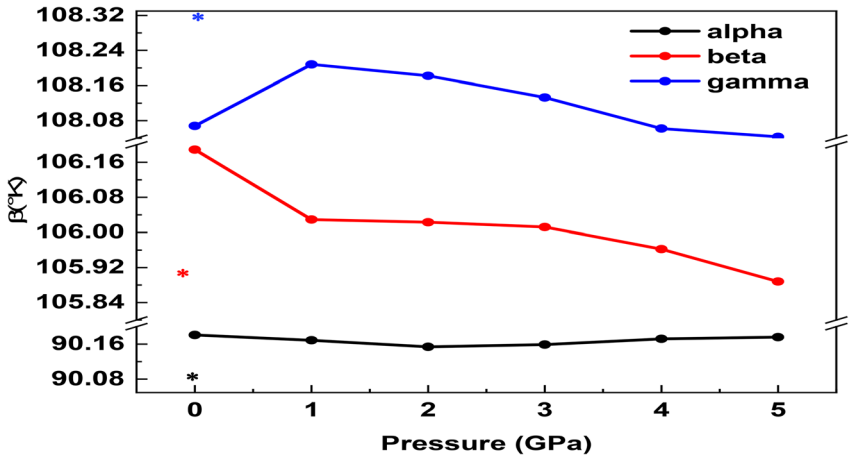

Fig. 9 β(*K*) as a function of pressure for the three polymorphs (α, β, γ)-$C_9H_{17}NO_2$.

respectively, for (α, β, γ)-$C_9H_{17}NO_2$ compounds. The reflectivity spectra as a function of photon energy are shown in Fig. 7. It starts with a value of ~0 eV for all the compounds. From there, it increases up to a maximum intensity of 19.37 eV, 20.00 eV and 20.21 eV for (α, β, γ)-$C_9H_{17}NO_2$, respectively, indicating that they are good candidates as coating materials in these energy ranges. It goes to zero at $E = 25$ eV. The behavior of light in a medium is described by the refractive index (n), which is a dimensionless quantity; it depends on the measurement wavelength (Fig. 8). The crystals absorb photon energy in the range of 0–10 eV. In the visible region, their absorption coefficient is low.

3.4. Beta angle as a function of pressure

In organic chemistry, planarity is an important concept because it can affect the reactivity and physical properties and can influence the stability and characteristics of a molecule. The molecules of the (α, β, γ)-$C_9H_{17}NO_2$ compounds are different from each other by symmetry. The beta angle plays a very important role in the stability and characteristics of the molecule. We studied the influence of pressure on beta angle, which in turn influences the physical properties of the molecule (Fig. 9). The beta angle decreases in the alpha and beta phases and increases in the gamma phase in the pressure range of 0–1 GPa, and the beta angle curve in the alpha phase is parabolic in the pressure range of 0–5 GPa and decreases gradually from 1 GPa in the beta and gamma phases.

4. Conclusion

Using density functional theory with pseudopotential plane waves within the generalized gradient approximation, this study provides a comprehensive analysis of the structural, electronic, and optical properties of the (α, β, γ)-$C_9H_{17}NO_2$ compounds. Ground-state properties, such as lattice parameters (calculated here for the first time) and electronic and optical properties, are determined. Unfortunately, there are only a few works available for comparing the properties calculated in this study. A qualitative assessment of the transition enthalpy (E) among the (α, β, γ)-$C_9H_{17}NO_2$ compounds indicates that the γ phase is more stable than the other two phases at 0 K. It is observed that all compounds maintained their semiconductor nature at the Fermi level, with band gaps of 4.73 eV, 4.55 eV and 4.37 eV, respectively. The absorption spectra reveal that the (α, β, γ)-$C_9H_{17}NO_2$ compounds are sensitive to the ultraviolet region. The beta angle decreases in the alpha and beta phases and increases in the gamma phase in the pressure range of 0–1 GPa, and the beta angle curve in alpha phase is parabolic in the pressure range of 0–5 GPa and decreases gradually from 1 GPa in the beta and gamma phases. Thus, this study can be used to explain why some patients show improvement following gabapentin intake and others do not show improvements or show partial improvements.

Authors statements

Conceptualization: K. Bouferrache, data curation: M.A. Ghebouli, formal analysis: Maroua I. Benamrani, Rabah Boudissa, validation: Faisal Katib Alanazi, M. Fatmi.

Conflicts of interest

The authors declare no potential conflicts of interest.

Data availability

Data underlying the results presented in this study are not publicly available at this time but may be obtained from the author (fatmimessaoud@yahoo.fr) upon reasonable request.

Acknowledgements

The authors extend their appreciation to the Deanship of Scientific Research at Northern Border University, Arar, KSA, for funding this research work through the project number NBU-FFR-2025-310-18.

References

1 R. Coelho and B. Aladenize, *Dielectrics: Dielectric Properties of Insulating Materials, Treatise on New Technologies, Materials Series*, Hermes, 1993, p. 230.
2 R. Bolinche, *Characterization of Surface and Volume Transport Phenomena of Electric Charges in Polymers, Doctoral Thesis*, Paul Sabatier University, Toulouse, 1997.
3 H. A. Reece and D. C. Levendis, Polymorphs of Gabapentin, *Acta Crystallogr. C*, 2008, **64**(3), 105–108.
4 J. A. Ibers, *Acta Crystallogr. C*, 2001, **57**, 641–643.
5 L. Magnus, *Epilepcia*, 1999, **40**, 66–72.
6 Y. Chang, *Étude de caractérisation de matériaux diélectriques de grille à forte permittivité pour les technologies CMOS ultimes*, Thèse de doctorat, INSA Lyon, France, 2003.
7 P. J. Gielisse, P. J. Gielisse, V. I. Ivanov-Omskii, G. Popovic, and M. Prelas, *Proc. 3rd Int. Symp. On Diamond Films*, St. Petersburg, 1996, pp. 281–296.
8 H. Holloway, H. C. Hass, M. A. Tamor, T. R. Anthony and W. F. Banholzer, *Phys. Rev. B*, 1991, **44**, 7123–7126.
9 F. Rebib, E. Tomasella, S. Aida, M. Dubois, E. Bêche, J. P. Gaston, J. Cellier and M. Jacquet, *Propriétés optiques et électriques de couches minces d'oxynitrure de silicium déposé par pulvérisation cathodique RF réactive*, Blaise Pascal University, 2006.
10 M. Feneberg, R. A. R. Leute, B. Neuschl, K. Thonke and M. Bickermann, *Phys. Rev. B*, 2010, **82**(7), 075208.
11 A. AlShaikhi and G. P. Srivastava, *J. Appl. Phys.*, 2008, **103**(8), 083554.
12 X. Gao, *et al.*, Electric-Field- and Stacking-Tuned Antiferromagnetic FeClF Bilayer, *Adv. Funct. Mater.*, 2025, **35**, 2417857.
13 J. Mejía-López, *et al.*, Two-Dimensional Intrinsic Half-Metals With Large Spin Gaps, *2D Mater.*, 2023, **10**, 045005.
14 S. J. Clark, *et al.*, *Z. Kristallogr.*, 2005, **220**, 567.
15 L. Krache, *et al.*, *Acta Phys. Pol. A*, 2023, **143**(3), 30.
16 R. Boudissa, *et al.*, *Biochem. Biophys. Rep.*, 2024, **37**, 101601.
17 B. Ghebouli, *et al.*, *Acta Metall. Sin.*, 2011, **24**, 255.
18 S. R. Hall, F. H. Allen and I. D. Brown, *Acta Crystallogr. A*, 1991, **47**, 655–685.
19 F. Tran and P. Blaha, *Phys. Rev. Lett.*, 2009, **102**, 226401, DOI: **10.1103/PhysRevLett.102.226401**.
20 D. Li, F. Ling, Z. Zhu and X. Zhang, *Physica B*, 2011, **406**, 3299.
21 Y. Fang, *et al.*, *J. Phys. Chem. Solids*, 2019, **127**, 107–114.
22 M. Zhong, *et al.*, *J. Phys. Chem. Solids*, 2018, **121**, 139–144.
23 M. Jubair, *et al.*, *J. Phys. Commun.*, 2019, **3**, 055017.